Validation of Computational Fluid Dynamics Models for Evaluating Loose-Fitting Powered Air-Purifying Respirators

Michael Bergman(✉), Zhipeng Lei, Susan Xu, Kevin Strickland, and Ziqing Zhuang

National Personal Protective Technology Laboratory,
National Institute for Occupational Safety and Health,
Pittsburgh, PA 15236, USA
mbergman@cdc.gov

Abstract. Loose-fitting powered air-purifying respirators (PAPRs) are used in healthcare settings to reduce exposure to high-risk respiratory pathogens. Innovative computational fluid dynamics (CFD) models were developed for evaluating loose-fitting PAPR performance. However, the computational results of the CFD models have not been validated using actual experimental data.

Experimental testing to evaluate particle facepiece leakage was performed in a test laboratory using two models of loose-fitting PAPRs. Each model was mounted on a static (non-moving) advanced headform placed in a sodium chloride (NaCl) aerosol test chamber. The headform performed cyclic breathing via connection to a breathing machine. High-efficiency particulate air (HEPA)-filtered air was supplied directly to the PAPR facepiece using laboratory compressed supplied-air regulated with a mass-flow controller. One model was evaluated with six supplied-air flowrates from 50–215 L/min (Lpm) and the other model with six flowrates from 50–205 Lpm. Three different workrates (minute volumes) were evaluated: low (25 Lpm), moderate 46 (Lpm), and high 88 (Lpm). Manikin penetration factor (mPF) was calculated as the ratio of chamber particle concentration to the in-facepiece concentration.

Overall, data analyses indicated that the mPF results from the simulations were well correlated with the experimental laboratory data for all data combined ($r = 0.88$). For data at the three different workrates (high, moderate, low) for both models combined, the r-values were 0.96, 0.97, and 0.77, respectively. The CFD models of the two PAPR models were validated and may be utilized for further research.

Keywords: Powered air-purifying respirators · PAPR · CFD
Manikin penetration factor

1 Introduction

Loose-fitting powered air-purifying respirators (PAPRs) use a battery powered motorized fan to draw air through an air-purifying element (particulate filter and/or sorbent cartridge) and supply it to a loose-fitting facepiece (forming a partial seal to the

S. Bagnara et al. (Eds.): IEA 2018, AISC 819, pp. 176–185, 2019.
https://doi.org/10.1007/978-3-319-96089-0_20

face) or hood (completely covering the head and neck and may also incorporate a shroud to cover portions of the shoulders and torso). Because loose-fitting PAPRs do not incorporate a tight seal to the face, they do not require fit testing. Interest in their use is becoming more prevalent in healthcare settings [1].

For use in the U.S., PAPRs are designed to meet National Institute for Occupational Safety and Health (NIOSH) certification requirements which were developed based on industrial use [2]. The supplied-air flowrates of loose-fitting PAPRs available on the market are in the range of 170–206 Lpm [3], while peak inhalation flows of adults exercising at heavy workloads can be 255 Lpm [4]. Gao et al. [5] mounted loose-fitting PAPRs on a manikin and measured the protection levels when the manikin breathed at varying workloads (mean inhalation flowrate): low (30 Lpm), medium (55 Lpm), high (85 Lpm), and strenuous (135 Lpm). The protection levels at the high and strenuous workloads were significantly lower than the ones at the other workloads.

Computational Fluid Dynamics (CFD) methods are computerized models which can evaluate the performance of respiratory protective equipment, e.g., N95 filtering facepiece respirators [6, 7]. Lei et al. [8] simulated the performance of loose-fitting PAPRs on a headform using CFD simulations and determined the effects of breathing workloads and supplied-air flowrates on the PAPR's performance. However, the computational results of the CFD models have not been validated using actual experimental data. The objective of this study was to collect and use actual experimental data to validate the CFD PAPR models. The CFD models and experimental methods evaluated PAPR performance at varied workrates and supplied-airflows to the PAPR facepiece.

2 Methods

2.1 PAPR Models

Two loose-fitting PAPR models currently used by healthcare workers were evaluated: MaxAir® 78SP-36 with disposable cuff (size S/M) (Bio-Medical Devices, Inc., Irvine, CA) and the 3M Air-Mate™ with BE-12 facepiece (size regular) (3M Company, St. Paul, MN). Both models have an assigned protection factor (APF) of 25 as designated by the U.S. Occupational Safety and Health Administration (OSHA) [9] (Fig. 1). The MaxAir® is a helmet design, with a blower motor and filter contained within the helmet. The motor draws outside air through a HEPA filter and blows the purified air into the facepiece. It has three airflow settings, tested in our laboratory as low (191 Lpm), medium (214 Lpm), and high (237 Lpm) using a test system described by Bergman et al. [10]. For our experiments, the blower motor was removed from the PAPR and replaced with a tube connected to a source of HEPA-filtered supplied air from the laboratory compressor system (further described in Sect. 2.1). A hole was drilled into the helmet and the tube was inserted through the hole; silicone sealant was then used to seal the interface. The tube bypassed the PAPR's filter and delivered the supplied-air directly into a cavity in the helmet. From this cavity, the air then flowed into the facepiece area.

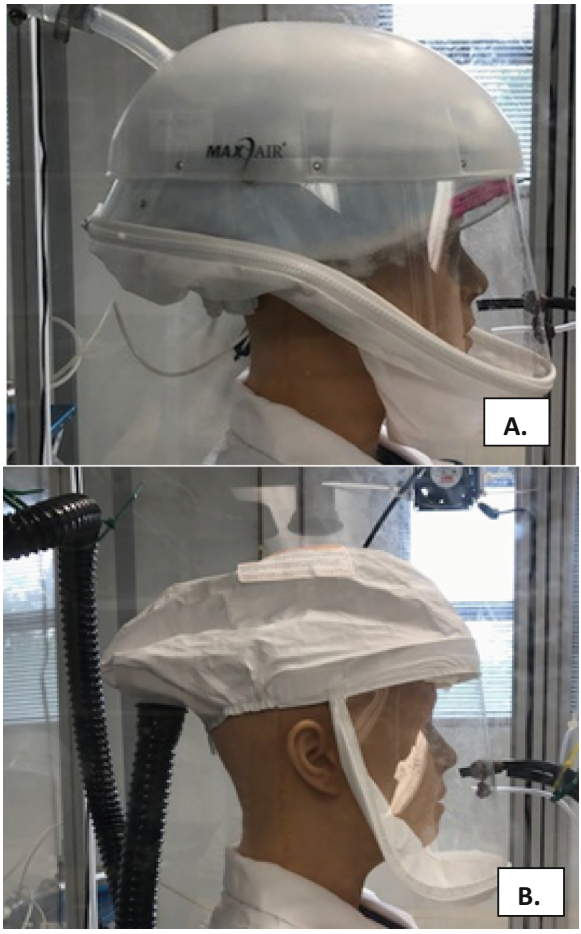

Fig. 1. PAPR models. (A) MaxAir® 78SP-36 Cuff System with disposable cuff (size S/M) (Bio-Medical Devices, Inc., Irvine, CA); (B) 3M Air-Mate™ with BE-12 facepiece (size regular) (3M Company, St. Paul, MN)

The Air-Mate™ is designed with an external blower containing a HEPA filter; a hose connects the blower unit to the facepiece. The facepiece has an elastic neck cuff design. The Air-Mate™ has only one airflow setting (measured at 211 Lpm). For modification of our testing, the exterior blower and filter were not used; the PAPR's hose was connected directly to the filtered laboratory supplied-air system.

CFD Simulations

We modeled the two loose-fitting PAPR systems by 3D scanning and surface processing. In the CFD models, the digital scan of the PAPR was donned on the digital image of the static advanced headform. We then modeled the interior volume of the PAPR. Figure 2 shows the CFD model of the headform and MaxAir® PAPR; the model comprises the breathing zone and the boundaries that include the PAPR interior

surface, headform surface, walls of the breathing airway, supplied-air venting holes which direct air towards the face, and the volume of the loose-fitting area around the neck. We further meshed the CFD model into hexahedral cells using ANSYS ICEM software (ANSYS 2018, Ansys, Inc., Pittsburgh, PA). A CFD model using the AirMate™ PAPR was also similarly constructed.

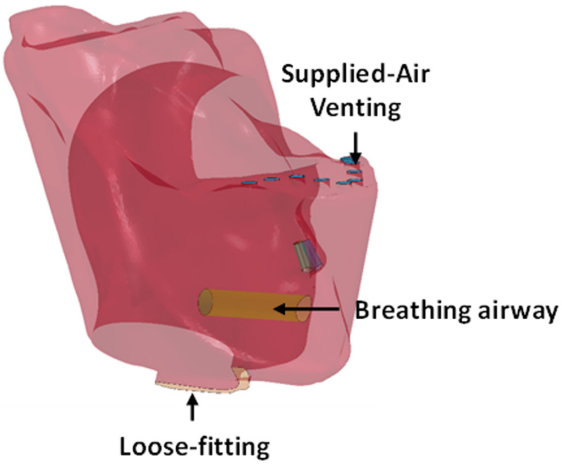

Fig. 2. The CFD model of the headform/MaxAir® PAPR volume

A time-dependent flowrate with a sine wave shape was applied to the inlet of the breathing airway to simulate a cyclic breathing pattern (inhalation and exhalation). A constant flowrate with the direction towards the PAPR breathing zone was applied to the supplied-air venting holes. For both PAPR models, three different workrate minute volumes were tested: low (25 Lpm), moderate (46 Lpm), and high (88 Lpm). One model was tested with supplied-air flowrates from 50–215 Lpm; the other model was tested with supplied-air flowrates from 50–205 Lpm. The loose-fitting area is the pressure outlet boundary where air flowed out of the PAPR. The flow velocity at the surfaces of the headform, breathing airway and PAPR were held at zero (i.e., non-slip boundary conditions were used).

The pisoFoam solver (in OpenFOAM) with the PISO (Pressure Implicit with Splitting of Operators) algorithm was used to perform the CFD simulation because we assumed that the flow is transient and incompressible and has a turbulent effect. Each simulation calculated a 20 s time duration with a 0.001-second time-step; at each time step, the pressure field and the velocity field inside the PAPR breathing zone were determined. Only one simulation run was performed for each supplied-air flowrate/workrate combination; multiple runs would have resulted in negligible variance of results.

The challenge particles, which were the particles outside of the PAPR model, were evenly placed at the gap of the loose-fitting area. At every 0.001-second time-step, particles with size 0.1 μm and concentration 100,000 particles/cm^3 were virtually generated. The tool for the Lagrangian particle tracking in OpenFOAM software

calculated the particles that leaked into the facepiece. The interaction between particles and wall boundaries was tracked. We assumed that a particle would stick to a wall boundary after the impact happens between them. Each CFD simulation also determined movements of all particles, which were used to calculate the particle concentration of the inhalation airflow at the opening of the mouth during the entire 20 s simulation time.

Supplied-Air System (Experimental Testing)

Air from the laboratory compressor system was first regulated and then flowed to a mass flow controller (model: 5853, Brooks Instrument, Hatfield, PA) using a microprocessor controller and readout unit (model: 0154, Brooks Instrument, Hatfield, PA). This setup allowed the test operator to easily set a continuous flowrate. Downstream of the mass flow controller, the air passed through a HEPA filter (model: Air-Mate^{TM} filer p/n 451-02-01R01, 3M Inc.) mounted in a test fixture. Before the air entered the PAPR, the flow rate was measured using a mass flow meter (model: HFM-D-301A, Teledyne Hastings Instruments, Hampton, VA) with a digital readout (model: THCD-100, Teledyne Hastings Instruments, Hampton, VA) (Fig. 3).

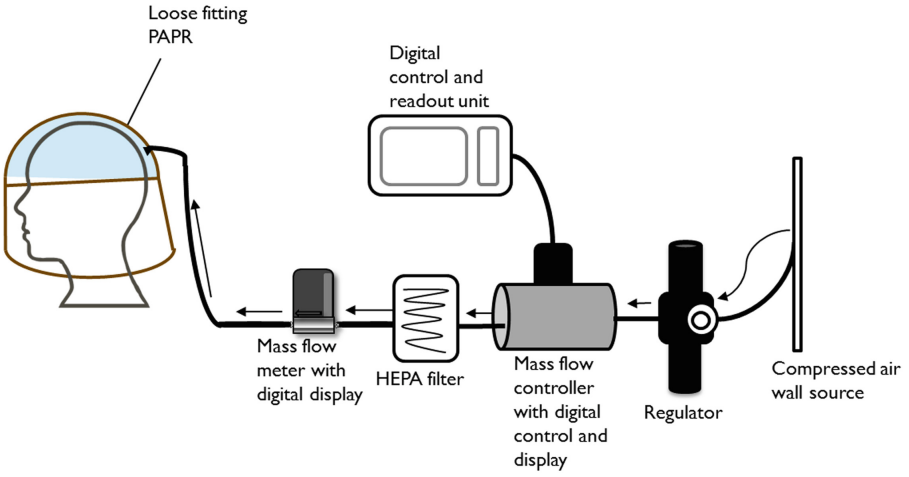

Fig. 3. Supplied-air test setup

NaCl Test Chamber (Experimental Testing)

The facepiece particle leakage for both PAPR models was tested in an acrylic test chamber (l, w, h: 30” × 36” × 72”) equipped with mixing fans and an exhaust port. PAPR facepieces were mounted onto a medium-sized static advanced headform described by Bergman et al. [11]. The headform was connected to an external breathing lung with an inflatable bladder by a 22 mm inner diameter tube that travelled from the inside of the headform’s mouth to the inflatable bladder. A port on the breathing lung was connected via a hose to breathing simulator (model: BRSS, Koken Ltd., Japan).

The breathing simulator used a cyclic sinusoidal breathing pattern to inflate and deflate the bladder inside the breathing lung by changing the lung's internal pressure.

Sodium chloride (NaCl) aerosol was generated as the challenge aerosol using air from the laboratory compressor system. The airflow was directed through a six-jet Collison (BGI Incorporated, Waltham, MA) with 2 w/v % NaCl solution in deionized water. The aerosol then flowed through a diffusion drier (model: 3062, TSI, Inc., Shoreview, MN) and a Kr-85 neutralizer (model: 3054, TSI, Inc., Shoreview, MN) before entering the chamber. The chamber NaCl aerosol concentration was maintained between 2.0–2.5 $\times$ 10^5 particles/cm^3 by adjusting a separate supply line of HEPA-filtered dilution air (Fig. 3).

During five different test periods through the data collection, a size distribution analysis was run on the chamber aerosol using a scanning mobility particle sizer spectrometer (SMPS) (model: 3936, TSI Inc.) system consisting of a classifier controller (model: 3080, TSI, Inc.), a differential mobility analyzer (DMA) (model: 3081, TSI, Inc.), a condensation particle counter (CPC) (model: 377500, TSI, Inc.), and an aerosol neutralizer (model: 3077A, TSI, Inc.). Data from the five SMPS scans were averaged resulting in a count median diameter (CMD) of 60 nm with a geometric standard deviation (GSD) of 1.87 nm (Fig. 4).

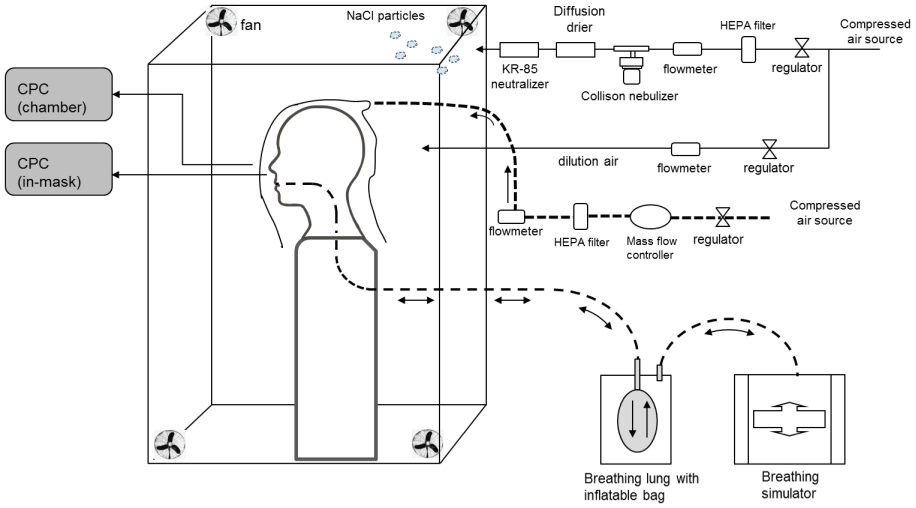

Fig. 4. Sodium chloride aerosol test chamber

Facepiece Leakage Measurements

Leakage measurements were taken using two condensation particle counters (CPC) (-model: 8022A; TSI, Inc.) and two laptop computers with Aerosol Instrument Manager® software (V.9.0.0.0, TSI, Inc.). One CPC sampled the chamber NaCl aerosol concentration (C_{out}) at a location $\sim$2 cm in front of the PAPR hood (i.e., outside of the hood) at the level of the headform's mouth. The other CPC sampled the NaCl aerosol concentration inside the facepiece (C_{in}) via the sample tube penetrating through the lens

of the facepeice. The model 8022A CPC has an accuracy of ±10% up to 5×10^5 particles/cm^3 as specified by the manufacturer. Both CPCs were set to sample in low flow mode (300 cm^3/min). Equal lengths of silicon conductive tubing were used to transport the aerosol to each CPC.

For each test, each CPC collected a 2-min sample at the rate of one data point/second. Five 2-min samples were taken in succession for each workrate/supplied-air flowrate combination. Each CPC reported the mean concentration of the 2-min sample which was later used for data analysis.

The average 2-min concentration of the chamber sample [C_{out}] was divided by the average 2-min concentration of the in-mask sample [C_{in}]; (Eq. 1).

$$\text{mPF} = [C_{out}]/[C_{in}] \tag{1}$$

Because the two models tested have an OSHA APF of 25, we limited mPF to a maximum of 10,000 for all data analyses. These calculated mPFs were then used to determine geometric mean (GM) mPFs and their geometric standard deviations (GSD) for the various workrate/supplied-air flowrate combinations.

JMP software (V.13, SAS Institute Inc., Cary, N.C.) was used to calculate the correlation coefficient (r-value) and the probability of significance (P-value) for comparison of GM mPF values from the experiments and the estimated mPFs from the CFD models. The r-value quantifies the strength and the direction of the relationship between two variables; if r is approaching +1, the two variables have a strong positive linear correlation. The P-value expresses the statistical significance of the correlation between the experimental GM mPFs and the estimated mPF value determined by the CFD simulation; we chose P-values <0.05 to define that there is a >95% probability that the two variables are significantly correlated.

3 Results

GM mPF experimental results and mPF CFD simulation results are plotted for different supplied-air flowrates and breathing workrates (Fig. 5). Figure 6 plots estimated mPFs determined in CFD simulations against GM mPFs measured in experiments. For all data combined from both models, the simulation results were well correlated with the experimental laboratory data (r = 0.88). For all data combined at the three different workrates (high, moderate, low), the r-values were 0.96, 0.97, and 0.77, respectively. All P-values assessing the correlation of GM mPF from the experiments and mPF from the CFD simulations were significant (P-value < 0.001) except for Model A at the low workrate (P-value > 0.05).

For Model A, the experimental GM mPFs and estimated mPFs were all 10,000 at the low workrate and supplied-air flow rates $\geq$ 75 Lpm; at supplied-air flow rates <75 Lpm, the experimental GM mPF results decreased to 100 while the simulation results remained at 10,000 (Fig. 5). At the moderate workrate and supplied-air flow rates of 50 and 205 Lpm, the experimental GM mPFs were 9 and 10,000 as compared to the

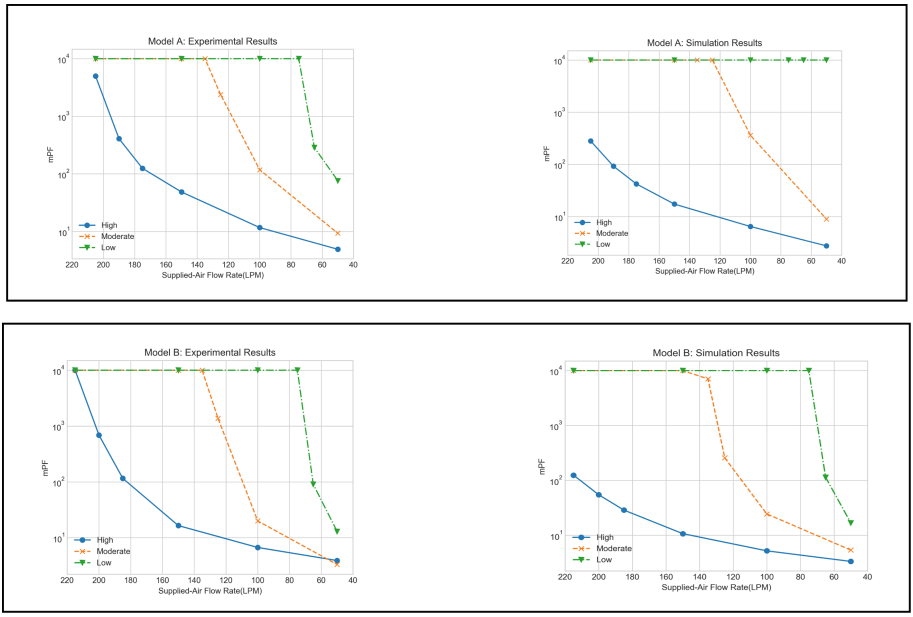

Fig. 5. GM mPF experimental and mPF estimated CFD simulation results by PAPR model at various supplied-air flowrates

estimated mPFs of 9 and 10,000. At the high workrate with supplied-air flow rates of 50 and 205 Lpm, the experimental GM mPFs were 5 and 4990 as compared to estimated mPFs of 3 and 205.

Model B results were similar to the trends for Model A (Fig. 5), with the distinction of Model B having better correlation of results for the low workrate (Fig. 6). The r-values for Model A plots in Fig. 6 are: 0.98, 0.98, and 0.0 for the high, moderate, and low workrates, respectively. The r-values for Model B plots in Fig. 6 are: 0.92, 0.98, and 1.0 for the high, moderate, and low workrates, respectively.

4 Discussion

The experimental results validated the CFD simulation results. The turbulent dispersion in airflows with high velocity may cause bias of mPF using the combination of high breathing workrate and high supplied-air flowrates. The particle diffusion in airflows with low velocity may be the origin of the differences in the experimental and estimated mPFs in Model A using the low breathing workrate and low supplied-air flowrates. Future studies will model the turbulent dispersion and the particle diffusion in CFD simulations of loose-fitting PAPRs.

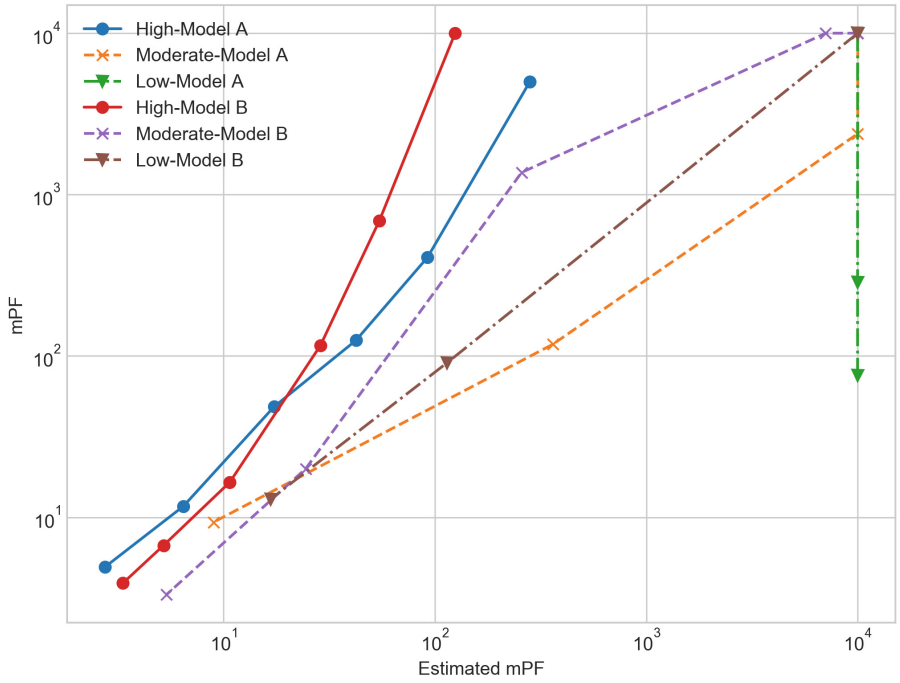

Fig. 6. Estimated mPF determined by CFD simulations versus GM mPF measured experimental results

5 Conclusion

Overall, data analyses indicated that the mPF results from the simulations were well correlated with the GM mPF experimental laboratory data for all data combined (R = 0.88). The CFD models of the two PAPR models were validated and may be utilized for further research. For data at the three different workrates (high, moderate, low) for both models combined, the r-values were 0.96, 0.97, and 0.77, respectively.

Further research can include more PAPR models and consider the impact of dynamic head and mouth movements on PAPR facepiece particle leakage. The CFD models for the two PAPR models were validated and may be applied in future PAPR performance research. Further research is needed to include more PAPR models and to consider the impact of human movements on PAPR particle leakage.

References

1. Wizner K, Stradtman L, Novak D, Shaffer R (2016) Prevalence of respiratory protective devices in US health care facilities: implications for emergency preparedness. Workplace Health Saf 64:359–368
2. Federal Register (1995) National Institute for Occupational Safety and Health (NIOSH). Respiratory protective devices. US Government Printing Office, Office of the Federal Register, Washington, DC. 42 CFR Part 84
3. Martin S, Moyer E, Jensen P (2006) Integrated unit performance testing of powered, air-purifying particulate respirators using a DOP challenge aerosol. J Occup Environ Hyg 3:631–641
4. Anderson NJ, Casidy PE, Janssen LL, Dengel DR (2006) Peak inspiratory flows of adults exercising at low, moderate and heavy work loads. J Int Soc Respir Prot 23:53–63
5. Gao S, McKay RT, Yermakov M, Kim J, Reponen T, He X, Kimura K, Grinshpun SA (2016) Performance of an improperly sized and stretched-out loose-fitting powered air-purifying respirator: manikin-based study. J Occup Environ Hyg 13:169–176
6. Lei Z, Yang J, Zhuang Z, Roberge R (2012) Simulation and evaluation of respirator faceseal leaks using computational fluid dynamics and infrared imaging. Ann Occup Hyg 57:493–506
7. Lei Z, Yang J (2014) Computing carbon dioxide and humidity in filtering facepiece respirator cavity during breathing cycles. In: ASME 2014 international design engineering technical conferences and computers and information in engineering conference. American Society of Mechanical Engineers, p V01AT02A077
8. Lei Z, Zhuang Z, Bergman M (2017) Application of digital human modeling for evaluating loose-fitting powered air-purifying respirators. In: Proceedings of the 5th international digital human modeling symposium
9. Federal Register (2006) Occupational Safety and Health Administration (OSHA). Assigned protection factors: Final rule. 29 CFR Parts 1910, 1915, 1926 71: 50121–50192
10. Bergman MS, Basu R, Lei Z, Niezgoda G, Zhuang Z (2017) Development of a manikin-based performance evaluation method for loose-fitting powered air-purifying respirators. J Int Soc Respir Prot 34(1):40–57
11. Bergman MS, Zhuang Z, Hanson D, Heimbuch BK, McDonald MJ, Palmiero AJ, Shaffer RE, Harnish D, Husband M, Wander JD (2014) Development of an advanced respirator fit-test headform. J Occup Environ Hyg 11(2):117–125